J Mater Sci (2009) 44:2890–2898
DOI 10.1007/s10853-009-3382-2

Photocatalysis for water oxidation by Fe_2O_3 nanoparticles embedded in clay compound: correlation between its polymorphs and their photocatalytic activities

Seiji Kakuta · Toshiyuki Abe

Received: 19 November 2008 / Accepted: 3 March 2009 / Published online: 25 March 2009

Abstract Iron oxide (Fe_2O_3) nanoparticles of distinct polymorphs (i.e., α and amorphous phases) were prepared in montmorillonite (MT) particularly with three types of methods (i.e., calcining, hydrothermal reaction, and hydrolysis) and used as photocatalysts for the oxidation of water to O_2. Although α-Fe_2O_3 has usually been applied to a photocatalysis system [employing the saturated loading of α-Fe_2O_3 (25 wt%) in MT], this study first showed that amorphous Fe_2O_3 has similar photocatalysis ability to α-Fe_2O_3 in terms of water oxidation. Moreover, irrespective of the types of polymorphs, their photocatalyses were dependent on the loading amount of Fe_2O_3 in MT; that is, the O_2 amount increased with the amount of the photocatalyst employed until the loading amount reached ca. 3 wt%, and decreased in the larger loading amount. In this article, the reason why such an optimal photocatalysis condition appears was considered in terms of kinetic aspects.

Introduction

Great efforts have been made to prepare an active photocatalyst for water splitting and pollutant decomposition [1]. Currently, photocatalyst fabrications are passively conducted particularly in view of an efficient uptake of visible-light energy into output. Among the conventional photocatalysts working under visible-light irradiation, iron oxide (Fe_2O_3) has been attracting attention as a potential photocatalyst because it is stable, safe, and inexpensive [2, 3]. Its various types of polymorphs such as α, β, γ, and amorphous have been recognized; however, only α-Fe_2O_3 has usually been used as photocatalyst [4–7]. The photocatalytic activity of α-Fe_2O_3 was found to depend on its particle size [6, 7]. This is because its photogenerated carriers have a short-diffusion length (<20 nm [4, 8]). Therefore, the study of the fabrication of fine-Fe_2O_3 particles has been conducted with an aim to establish an efficient photocatalysis system. Recently, Grätzel and colleagues [9] have reported the photocatalytic oxidation of water by dendritic α-Fe_2O_3 nanoparticles of 10 to 20 nm diameter. The use of a clay compound as a photocatalyst supporter was also effective for fabricating nanostructured α-Fe_2O_3 [10, 11]; the compound suppressed the nanoparticle aggregation. It has been known that α-Fe_2O_3 embedded in clay exhibits efficient photocatalytic activity for the decomposition of acetic acid into methane (called the photo-Kolbe reaction), which is superior to neat Fe_2O_3 in the photocatalytic activity [12, 13].

In general, an amorphous compound has not so far been applied to photocatalysis system. This is attributed to low carrier mobilities in amorphous compounds, resulting in inefficient photocatalysis. However, a few examples have recently been reported on amorphous photocatalysts (such as TiO_2 and Ta_2O_5) capable of water splitting [14, 15]. For instance, Domen and colleagues [15] have shown that the photocatalytic activity of amorphous Ta_2O_5 is higher than that of crystallized Ta_2O_5. The effectiveness of amorphous Ta_2O_5 originates from its mesoporous structure (pore size, ca. 1.8 nm; thickness, 4.4 nm) that reduces carrier recombination. With regard to amorphous Fe_2O_3, its photocatalytic activity has not been studied in detail. Amorphous Fe_2O_3 can

S. Kakuta · T. Abe (✉)
Department of Frontier Materials Chemistry, Graduate School of Science and Technology, Hirosaki University, 3 Bunkyo-cho, Hirosaki 036-8561, Japan
e-mail: tabe@cc.hirosaki-u.ac.jp

S. Kakuta
Aomori Industrial Research Center, 4-11-6, Daini-Tonyamachi, Aomori 030-0113, Japan

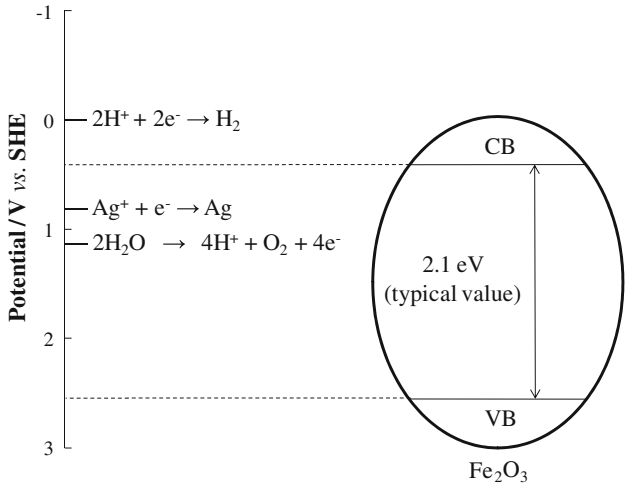

Scheme 1 Energy levels of Fe_2O_3 as well as the reactions concerned in the present study. VB and CB denote the valence and conduction bands, respectively

be prepared through aggregation of precursors [i.e., Fe(III)-hydroxy complexes such as $Fe^{III}(OH)^{2+}$ and $Fe^{III}(OH)_2^+$] under weakly acidic and alkaline conditions, which usually results in the formation of large particles [16, 17]. Such an amorphous species is known as hydrous ferric oxide (HFO) ($Fe_2O_3 \cdot xH_2O$), having a similar chemical structure to α-Fe_2O_3; thus, amorphous Fe_2O_3 may also be photocatalytically active. That is, an efficient photocatalysis system of amorphous Fe_2O_3 may be created, particularly by controlling the particle size at the nanometer scale.

In this study, Fe_2O_3 was synthesized in montmorillonite (MT) using different preparation methods, through which the authors successfully fabricated the nanoparticles of distinct polymorphs (i.e., α and amorphous phases). The photocatalytic activities of Fe_2O_3 loaded in MT were investigated through the multielectron transfer oxidation of water to O_2 (Scheme 1), where the photocatalysis of Fe_2O_3 for O_2 evolution is examined in terms of the types of its polymorph and loading amount in the clay. As a result, this study involved the first finding that the photocatalysis ability of amorphous Fe_2O_3 is comparable to that of α-Fe_2O_3. This article also describes the factors affecting the photocatalysis of Fe_2O_3 for water oxidation.

Experimental

Purification of MT, and preparation of Na^+-type MT

An aliquot of 20 g of bentonite clay (Nihon Koken, Tsugaru-2) was introduced into 0.9 dm^3 of deionized water; subsequently, 0.1 dm^3 of 3% hydrogen peroxide solution was added into the suspension for removing organic matters from the clay. The suspension was stirred for 5 h, after which MT was isolated from bentonite by means of centrifugation. The obtained MT was soaked in 1.0 dm^3 of 1 mol dm^{-3} NaCl solution, through which the cation-exchange sites in the MT were replaced by Na^+ (this treatment was repeated thrice). The resulting Na^+-type MT was washed with deionized water and dried at 100 °C. As a result, ca. 7 g of Na^+-type MT was obtained.

Preparations of photocatalyst embedded in MT

Fe_2O_3 was loaded into Na^+-type MT using three types of methods (i.e., calcining, hydrothermal reaction, and hydrolysis).

Method a: Trinuclear acetato-hydroxo iron (III) nitrate ($[Fe_3O(OCOCH_3)_7OH \cdot 2H_2O]NO_3$) was prepared from iron(III) nitrate enneahydrate (Kanto Chemical) and acetic anhydride (Wako Pure Chemical), according to a previous procedure [10]. An aqueous complex solution (0.1 mol dm^{-3}) was prepared and quickly dropped into a suspension (0.1 dm^3) of 1 wt% Na^+-type MT with stirring (the additive amount of the complex solution changes with the loading amount of Fe_2O_3 in MT), after which the mixture was stirred for 5 h at room temperature. The product was washed with deionized water and dried on a glass plate at room temperature, followed by calcining at 400 °C under air (for 10 h). The saturated amount of Fe_2O_3 in MT was ca. 25 wt%. The Fe_2O_3 loaded in MT through calcining is denoted as CL-Fe_2O_3/MT. As a reference, neat Fe_2O_3 (denoted as CL-Fe_2O_3) was also prepared according to the above-mentioned procedure and used as-prepared.

Method b: The $[Fe_3O(OCOCH_3)_7OH \cdot 2H_2O]NO_3$ solution (0.1 mol dm^{-3}) was dropped into a suspension of 1 wt% Na^+-type MT with stirring, followed by continuous stirring for 5 h (the additive amount of the complex solution changes with the Fe_2O_3 amount in MT, similar to method a). The resulting mixture solution was put into a gas-tight glass vessel and aged for 3 days in an oven at 120 °C. The resulting product (denoted as HT-Fe_2O_3/MT) was washed with deionized water and dried at room temperature. As a reference, neat HT-Fe_2O_3 was also prepared by means of the hydrothermal reaction with 0.5 mol dm^{-3} of aqueous $[Fe_3O(OCOCH_3)_7OH \cdot 2H_2O]NO_3$ solution.

Method c: An aqueous solution of $Fe(NO_3)_3 \cdot 9H_2O$ (0.1 mol dm^{-3}) was dropped into 0.1 dm^3 of 1 wt% Na^+-type MT suspension with stirring (the additive amount of the complex solution was controlled with the Fe_2O_3 amount in MT, similar to the methods a and b), and the resulting mixture solution was continuously stirred for 5 h at room temperature. The resulting Fe^{III}-type MT was first washed with deionized water in order to remove nitrate and thereafter put back into deionized water. The formation of

HFO in MT (HFO/MT) was carried out through hydrolysis, wherein 0.1 dm^3 of an aqueous NaOH solution (1 mol dm^{-3}) was added into 0.1 dm^3 of the Fe^{III}-type MT suspension. The resulting suspension (conc., 10.5 g dm^{-3}) of 5 wt% HFO/MT was washed with deionized water, and the product was stored in deionized water at room temperature. The saturated amount of HFO/MT was ca. 8 wt%.

Characterization of photocatalysts

The loading amount of Fe_2O_3 (or HFO) in MT was determined by thermogravimetry (Rigaku, TG-8120) at 400 °C under air (for 10 h). The specific surface area of the photocatalyst was determined using the Brunauer–Emmet–Teller method (Shimadzu-Micromeritics, FlowSorb II 2300). The polymorph of the photocatalyst part embedded in MT was identified by electron diffraction. A transmission electron microscope (TEM; Hitachi, H-8000) was operated at 200 kV for obtaining the sample images. For recording TEM images, ca. 0.1 g dm^{-3} of the suspension of the photocatalyst embedded in MT was prepared. A 1.0×10^{-5} dm^3 portion of the suspension was dropped onto a microgrid supported on a copper grid mesh (Nisshin EM, MJD02A) and dried at room temperature. A diffuse reflectance spectrum was measured using a UV–Vis spectrophotometer (JASCO, V-570) equipped with an integrating sphere (JASCO, ISN-470). For the measurement of a diffuse reflectance spectrum of Fe_2O_3 (or HFO) embedded in MT, 1 wt% of the suspension of photocatalyst (i.e., 3 wt% CL-Fe_2O_3/MT, 3 wt% HT-Fe_2O_3/MT, or 3 wt% HFO/MT) was prepared. A 1×10^{-3} dm^3 portion of the suspension was filtered. The photocatalysts were dried at room temperature and used as the samples for diffuse reflectance spectral measurement. The size distributions of neat HT-Fe_2O_3 particles were also measured by a dynamic light-scattering particle-size analyzer (HORIBA, LB-550), in addition to TEM imaging.

Photocatalytic experiments

The photocatalytic water oxidation was conducted in an aqueous Ag_2SO_4 solution [30 mmol dm^{-3} (pH = 6.2)] containing a known amount of a photocatalyst within an Ar atmosphere. The amount of the photocatalyst embedded in MT was varied while maintaining the amount of MT constant (20 mg). A 150-W halogen lamp was used as a light source (light intensity, 357 mW cm^{-2}) under typical conditions. For measuring the action spectrum for O_2 evolution, a tunable pulse laser (Hamamatsu Photonics, L5996) was used as the monochromatic light source (light intensity, 100 mW cm^{-2}). The light intensity was measured using a power meter (Gentec, PSV-3103V2). Gaseous products were analyzed by a thermal conductivity detector gas chromatograph (Shimadzu, GC-2010) with a capillary column (Molecular Sieve 5A) and Ar carrier gas.

Results and discussion

The structural characteristics of CL-Fe_2O_3/MT, HT-Fe_2O_3/MT, and HFO/MT were identified in terms of TEM images, specific surface areas, and diffuse reflectance spectra.

Figure 1 shows the TEM images of Fe_2O_3 (or HFO) embedded in MT and the corresponding electron diffraction patterns (inset) for different loading amounts of the photocatalysts. The d-spacing data obtained from electron diffraction spots are also summarized in Table 1. Figure 2 shows the size distributions of Fe_2O_3 and HFO particles, based on the TEM observations. The average size of Fe_2O_3 particles in 3 and 25 wt% CL-Fe_2O_3/MT was ca. 20 nm (Figs. 1a, b and 2a). The diffraction pattern of 25 wt% CL-Fe_2O_3/MT indicated that the polymorph of Fe_2O_3 is assignable to the α phase (Fig. 1a, Table 1) [18]. However, for <5 wt% of the loading amount (Fig. 1b), the electron diffraction spots from crystalline Fe_2O_3 were not observed, where the resulting diffraction pattern is consistent with that of the MT particles (Table 1). Figure 1b evidently exhibits that an amorphous phase of CL-Fe_2O_3 can be formed under the lower loading condition. Although the saturated loading of CL-Fe_2O_3 in MT (i.e., 25 wt% of CL-Fe_2O_3/MT) has usually been employed for photocatalyst applications [12, 13], the present result reveals that the polymorphs of CL-Fe_2O_3 depend on its loading amount.

In 3 and 25 wt% HT-Fe_2O_3/MT, the size of Fe_2O_3 particles was ca. 60 nm (Figs. 1c, d and 2b). The electron diffraction patterns were indicative of the α phase of Fe_2O_3, irrespective of the loading amount (Fig. 1c, d, Table 1). HFO has been recognized as amorphous Fe_2O_3 [16]. As depicted in Fig. 1e and f, and Table 1, the polymorph of HFO was characterized to be the amorphous phase through the electron diffraction patterns, similar to the 3 wt% CL-Fe_2O_3/MT (cf., the particle size in 3 and 8 wt% HFO/MT was realized to be ca. 30 nm, Fig. 2c). The results shown in Fig. 1 exhibit that the polymorphs of Fe_2O_3 change with the preparation procedures.

The specific surface area of Fe_2O_3 (or HFO) in MT was found to increase with the loading amount from 169 m^2 g^{-1} (1 wt%) to 329 m^2 g^{-1} (25 wt%) in CL-Fe_2O_3/MT, from 142 m^2 g^{-1} (1 wt%) to 298 m^2 g^{-1} (25 wt%) in HT-Fe_2O_3/MT, and from 156 m^2 g^{-1} (1 wt%) to 223 m^2 g^{-1} (8 wt%) in HFO/MT (Fig. 3). This may exhibit that the aggregation of Fe_2O_3 (or HFO) can be suppressed by using an MT matrix as a supporter.

The diffuse reflectance spectra of Fe_2O_3 and HFO are shown in Fig. 4a. The absorption edge of CL-Fe_2O_3/MT, HT-Fe_2O_3/MT, and HFO/MT was at a wavelength of ca.

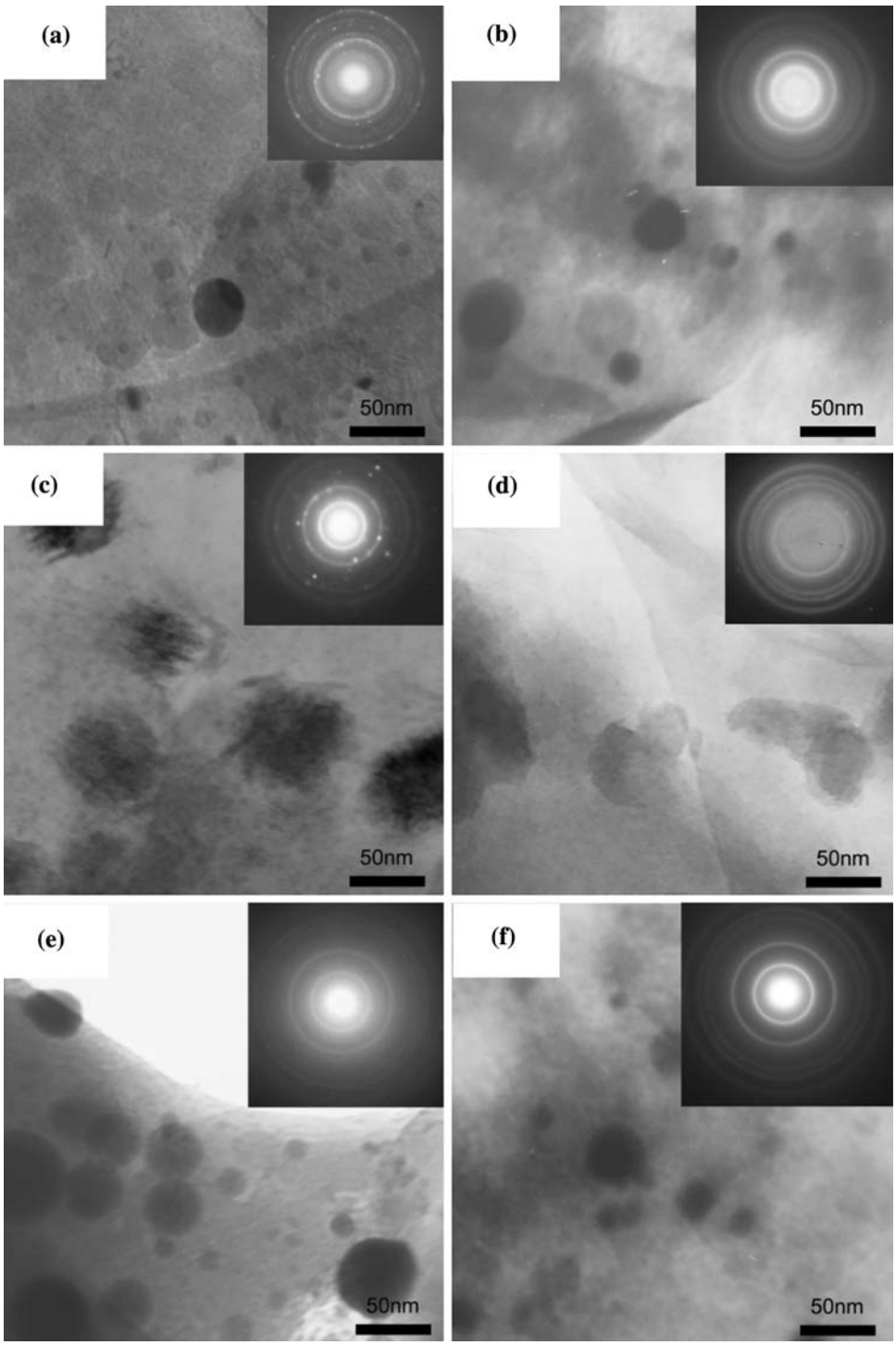

Fig. 1 TEM images and electron diffraction patterns (*inset*) of photocatalyst particles in MT. **a** 25 wt% CL-Fe_2O_3/MT, **b** 3 wt% CL-Fe_2O_3/MT, **c** 25 wt% HT-Fe_2O_3/MT, **d** 3 wt% HT-Fe_2O_3/MT, **e** 8 wt% HFO/MT, and **f** 3 wt% HFO/MT

600 nm. From the $\alpha^{1/2}$ versus $h\nu$ plots (Fig. 4b), the band gap energies of CL-Fe_2O_3/MT, HT-Fe_2O_3/MT, and HFO/MT were calculated to be 2.04, 2.09, and 2.02 eV, respectively. The band gap of α-Fe_2O_3 (in the absence of clay) has been reported to be 2.0–2.3 eV [19, 20], being in good agreement with the resulting values in this study. The chemical structure of amorphous Fe_2O_3 is essentially similar to that of α species (cf., the O^{2-} ion in amorphous Fe_2O_3 occupies the octahedral site of Fe^{3+} ion, in the same manner as α-Fe_2O_3) [21]; moreover, the absorption at around 600 nm can be induced through d–d transition in an Fe^{3+} ion [20, 22]. Therefore, it is reasonable that the band gap energies of Fe_2O_3 and HFO are independent of their polymorphs.

The photocatalytic activities of Fe_2O_3 and HFO for water oxidation were investigated in the presence of

Table 1 D-spacing obtained from electron diffraction pattern

D-spacing (nm)							
Na^+-type MT[a]	α-Fe_2O_3[b]	CL-Fe_2O_3/MT (wt%)		HT-Fe_2O_3/MT (wt%)		HFO/MT (wt%)	
		25	3	25	3	8	3
0.447		0.442	0.449	0.446	0.446	0.446	0.448
	0.369	0.366		0.371	0.370		
0.334		0.335	0.336	0.333	0.335	0.335	0.333
0.323		0.321	0.335	0.321	0.324	0.322	0.324
	0.270	0.266		0.269	0.268		
	0.252	0.252		0.251	0.251		
	0.221	0.221		0.220			
	0.184	0.184		0.185	0.186		
	0.170	0.168		0.168			

The measurement error for electron diffraction analysis was ±0.004 nm

[a] D-spacing of Na^+-type MT was determined by means of X-ray powder diffraction

[b] From Ref. [18]

Ag_2SO_4 (electron acceptor), in terms of the preparation methods of Fe_2O_3 and HFO (i.e., the types of polymorph) and the loading amount in MT.

First, the photocatalytic water oxidation by Fe_2O_3 (or HFO) was performed with and without an MT matrix. Table 2 shows the amount of the O_2 produced in each system. Irrespective of the types of its polymorph, Fe_2O_3 (or HFO) embedded in the clay yielded more O_2 than that yielded by the corresponding neat species. The present result also reveals that amorphous Fe_2O_3 (i.e., 3 wt% CL-Fe_2O_3 and HFO) is capable of photocatalytic O_2 evolution. In addition, it also appeared that CL-Fe_2O_3/MT exhibits similar activity to those exhibited by HFO/MT (amorphous phase) at the lower loading amount (3 wt%) and HT-Fe_2O_3/MT (α phase) at the higher loading amount (25 wt%); that is, the photocatalytic activity of a polymorph (α or amorphous) is independent of the preparation procedures. The results in Table 2 may be associated with a refining effect of photocatalyst particles by the use of the clay as a supporter. The particle size of neat CL-Fe_2O_3 and neat HFO was actually identified to be ≥10 μm from TEM observation; however, the particle size of neat HT-Fe_2O_3 was ca. 60 nm, which is comparable to that of HT-Fe_2O_3/MT. In order to investigate the difference between the photocatalytic activities of HT-Fe_2O_3/MT and neat HT-Fe_2O_3, the particle sizes of neat HT-Fe_2O_3 dispersed in deionized water and in an aqueous Ag_2SO_4 solution (30 mmol dm^{-3}) were measured using a dynamic light-scattering particle-size analyzer (Fig. 5). The particle size of HT-Fe_2O_3 dispersed in deionized water agreed with that estimated from its TEM image; however, that of neat HT-Fe_2O_3 dispersed in the aqueous Ag_2SO_4 solution was ca. 300 nm. Thus, neat HT-Fe_2O_3 was monodispersed in deionized water, while it exhibited aggregations in the Ag_2SO_4 solution. Metal oxide particles easily aggregate in an electrolyte solution due to a decrease in the zeta potential of the particle surfaces (i.e., the aggregation can be induced by the van der Waals force between the particles) [23, 24]. The present result evidently shows that a clay supporter can prevent the aggregation of the photocatalyst particles particularly in an Ag_2SO_4 solution; thus, the photocatalyst loaded in MT exhibits higher activity than the corresponding neat photocatalyst.

Figure 6 shows the time-course of the amount of the O_2 produced in HT-Fe_2O_3/MT (α) and HFO/MT (amorphous), which is measured with respect to the loading amount of the photocatalysts employed. It seemed that the amorphous species exhibits almost the same photocatalytic activity as the α species, as also indicated in Table 2. Moreover, the profiles of O_2 evolution were also independent of the types of polymorphs; that is, the O_2 amount increased with the amount of the photocatalyst employed up to ca. 3 wt% loading and decreased in the larger amount (cf., there was no confirmation of O_2 without irradiation, see Fig. 6). As shown in Fig. 2, it was confirmed for each photocatalyst sample that the size distributions of particles embedded in MT were almost independent of the loading amount. Therefore, it is most probable that the O_2 amount depends on the surface area of photocatalyst particles that varied with the loading amount of a photocatalyst (cf., Fig. 3). The oxidation of water into O_2 needs to take place through four-electron transfer; therefore, from the kinetic aspect, a high concentration of holes on the photocatalyst surface may be essential to the efficient evolution of O_2. The

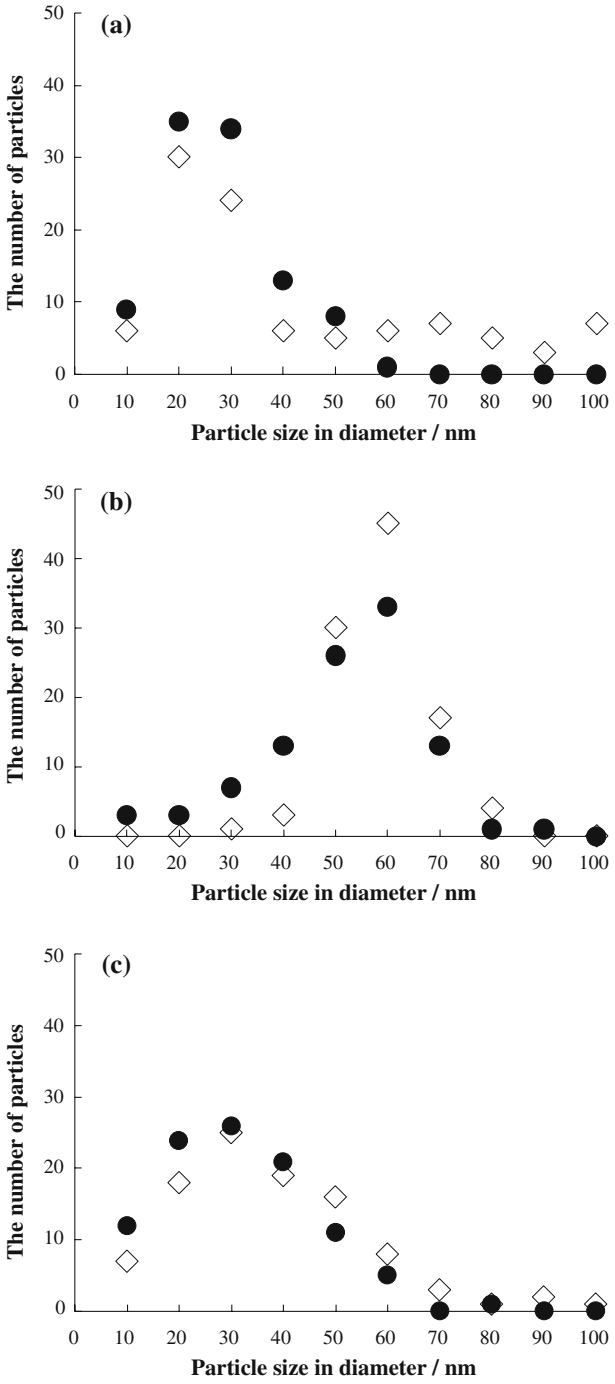

Fig. 2 Distributions of the size of Fe_2O_3 particles loaded into MT. **a** CL-Fe_2O_3/MT (◇, 25 wt%; ●, 3 wt%), **b** HT-Fe_2O_3/MT (◇, 25 wt%; ●, 3 wt%), and **c** HFO/MT (◇, 8 wt%; ●, 3 wt%)

present results are indicative of a decrease in the hole concentration with an increase in the number of active sites with the specific surface area (i.e., an interspersion of the active sites).

As has been reported previously, the photocatalytic water oxidation by α-Fe_2O_3 takes place according to the following equations [25].

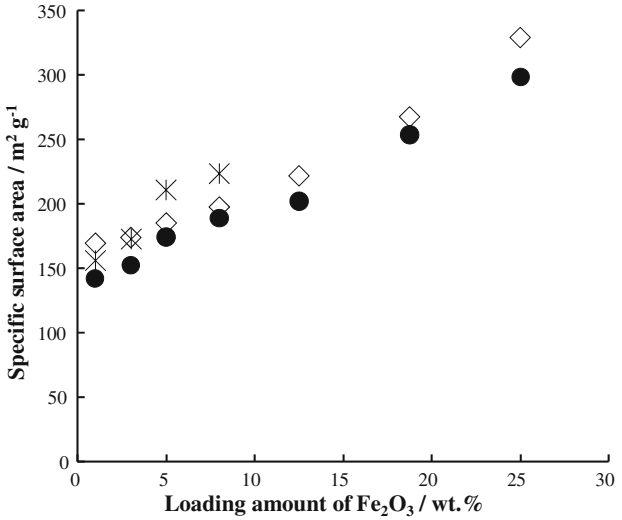

Fig. 3 Dependence of the specific surface area on the loading amount of photocatalyst (◇, CL-Fe_2O_3/MT; ●, HT-Fe_2O_3/MT; *, HFO/MT)

$$H_2O(ads) + h^+ \rightarrow OH^\bullet + H^+ \quad (1)$$

$$4OH^\bullet \rightarrow 2H_2O_2 \rightarrow 2H_2O + O_2 \quad (2)$$

To gain insights into the kinetics of photocatalytic water oxidation, the O_2 evolution in the presence of hydrogen peroxide (H_2O_2) was examined using HT-Fe_2O_3/MT (α) and HFO/MT (amorphous) as the photocatalysts. Figure 7 shows the time-course of the O_2 amount, where the photocatalytic O_2 evolution is conducted in the presence of 100 μmol dm^{-3} H_2O_2 (cf., the H_2O_2 concentration was controlled to be equal to the OH^- concentration at pH 10.0). The addition of H_2O_2 into the photocatalysis systems enhanced the initial rate of O_2 evolution, after which the O_2 evolution rate returned to that in the absence of H_2O_2 (cf., as for almost similar O_2 evolution rate under the distinct pH conditions between Figs. 4 and 7, it may suggest that the physicochemical environment around the photocatalyst sites surrounded by the MT network is independent of the pH of the electrolyte solution employed [26]). The O_2 amount in the initial region (∼0.25 h) was almost equal to the additive amount of H_2O_2; that is, it appeared that the rate for H_2O_2 oxidation is superior to that for water oxidation, irrespective of the kinds of the photocatalysts employed. A similar characteristic has been reported with a photoelectrode of α-Fe_2O_3 thin film [27], in which H_2O_2 is oxidized in tenfold rate of H_2O. The results of Fig. 7 indicate that the water oxidation on the photocatalyst surface is the rate-limiting process (Eq. 1); thus, the surface concentration of holes kinetically affects the photocatalysis of Fe_2O_3 (or HFO) for O_2 evolution (vide supra). As for the optimal photocatalysis under the condition of 3 wt% loading in MT (Fig. 6), the appearance of such an optimal condition in the rate-limiting surface reaction is attributed

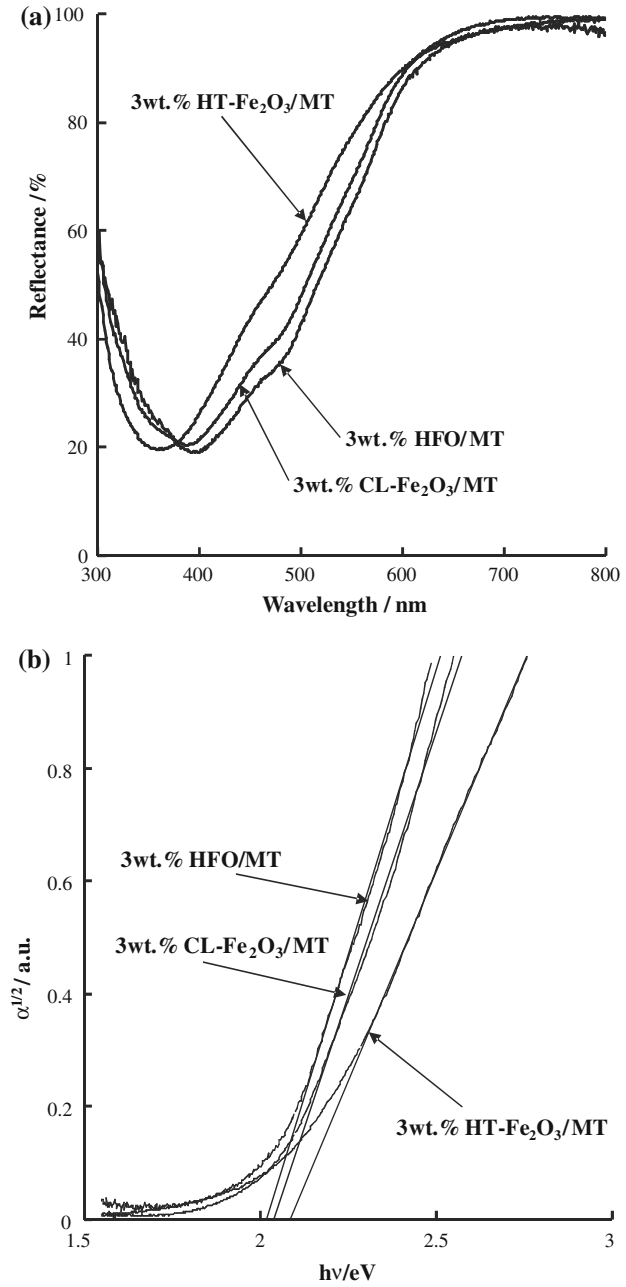

Fig. 4 **a** Diffuse reflectance spectra of 3 wt% CL-Fe_2O_3/MT, 3 wt% HT-Fe_2O_3/MT, and 3 wt% HFO/MT, and **b** estimation of the band gap energies

to a balance between the number of active sites and the hole concentration per the unit surface area.

The action spectra for O_2 evolution in 3 wt% HT-Fe_2O_3/MT and 3 wt% HFO/MT were examined (Fig. 8), where the amount of the O_2 produced at each wavelength was measured by irradiating tunable pulse laser for 3 h (cf., the light intensity was always constant at all the wavelengths, i.e., 100 mW cm^{-2}). Although the absorption edge of the photocatalysts employed is at around 600 nm (see Fig. 4),

Table 2 Typical photocatalysis data for O_2 evolution

Photocatalyst	The amount of the oxygen produced (μL)	
	With MT	Without MT[a]
3 wt% CL-Fe_2O_3 (amorphous)	71	17
3 wt% HT-Fe_2O_3 (α)	76	22
3 wt% HFO (amorphous)	79	11
25 wt% CL-Fe_2O_3 (α)	21	7
25 wt% HT-Fe_2O_3 (α)	19	6
None	0	0

The O_2 amount was quantified after the irradiation for 8 h

[a] The amount of the photocatalyst employed was the same as the corresponding MT-applied system (i.e., 0.6 mg at 3 wt% and 6.7 mg at 25 wt%)

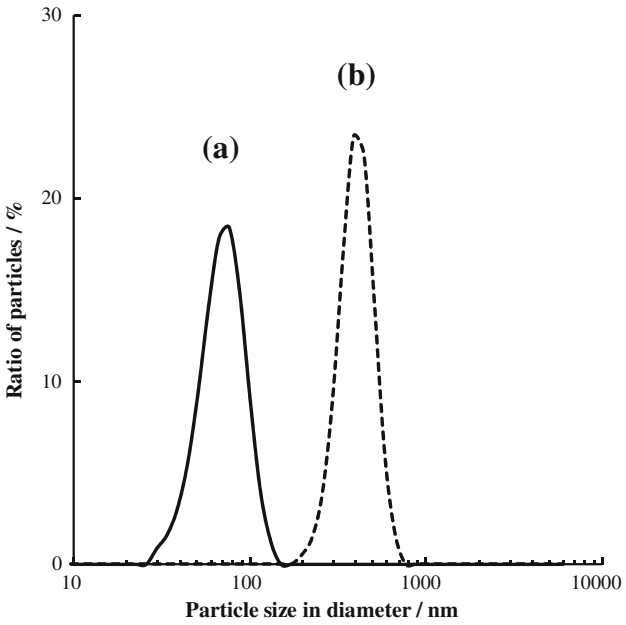

Fig. 5 Distributions of the size of neat HT-Fe_2O_3 particles in deionized water (a, *solid line*) and Ag_2SO_4 solution (b, *dotted line*)

O_2 was detectable at the wavelengths <550 nm. Recently, it has been reported that the lifetime of a charge transfer transition [from an Fe(III) ion to the nearest neighboring cation] in the range of <550 nm is longer than that of d–d transition (within an Fe(III) ion) in the range of 550 to 750 nm [22]. The present result reveals that amorphous Fe_2O_3 shows the photocatalysis through the same excitation process (i.e., charge transfer transition) as α-Fe_2O_3.

Conclusion

In this study, the photocatalytic activities of Fe_2O_3 and HFO were examined for water oxidation, in terms of the

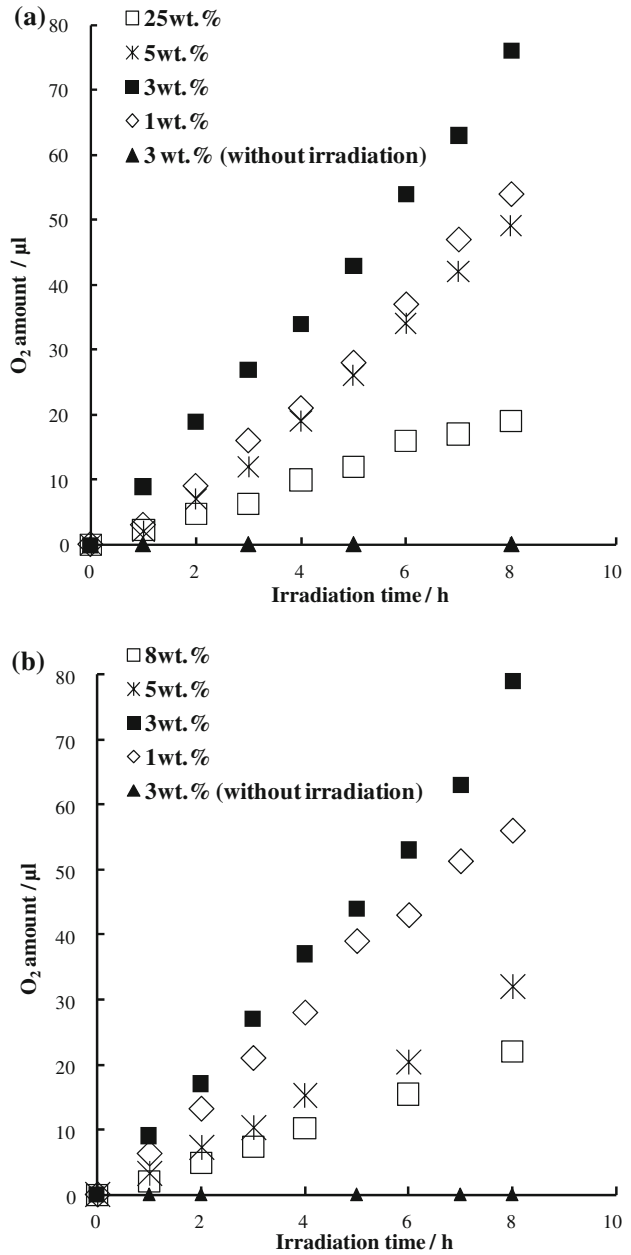

Fig. 6 Time-course of the amount of the O_2 produced in **a** HT-Fe_2O_3/MT (◇, 1 wt%; ■, 3 wt%; *, 5 wt%; □, 25 wt%; ▲, 3 wt% without irradiation), and **b** HFO/MT (◇, 1 wt%; ■, 3 wt%; *, 5 wt%; □, 8 wt%; ▲, 3 wt% without irradiation). Ag_2SO_4 concentration, 30 mmol dm^{-3} (pH = 6.2); light intensity, 357 mW cm^{-2}

types of their polymorphs and their loading amounts in a clay compound. The use of an MT matrix as a photocatalyst supporter was effective to the fabrication of Fe_2O_3 (or HFO) nanoparticles, which results in the active and efficient photocatalysis of Fe_2O_3 (or HFO) for O_2 evolution in comparison with the corresponding neat species. Although α-Fe_2O_3 (synthesized by calcining) has usually been applied to a photocatalysis system, particularly through its

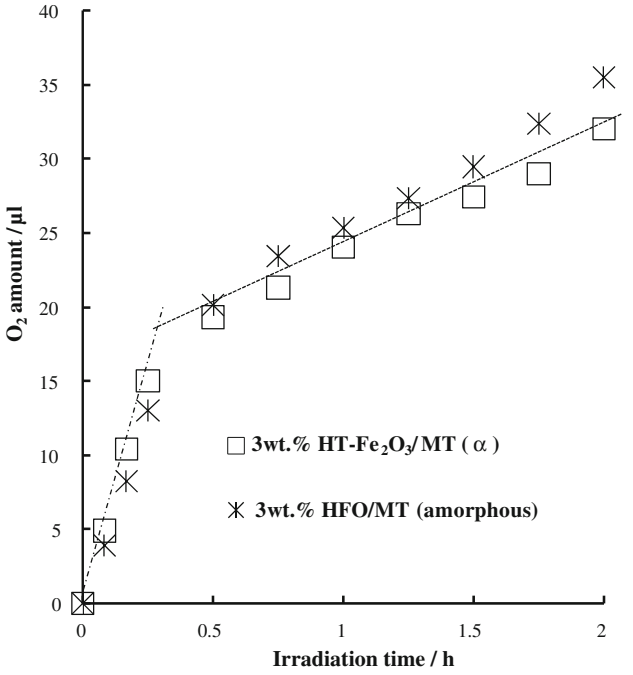

Fig. 7 Time-course of the O_2 amount in the presence of H_2O_2 (□, 3 wt% HT-Fe_2O_3/MT; *, 3 wt% HFO/MT). Ag_2SO_4 concentration, 30 mmol dm^{-3}; H_2O_2 concentration, 100 μmol dm^{-3}; pH = 6.2; light intensity, 357 mW cm^{-2}

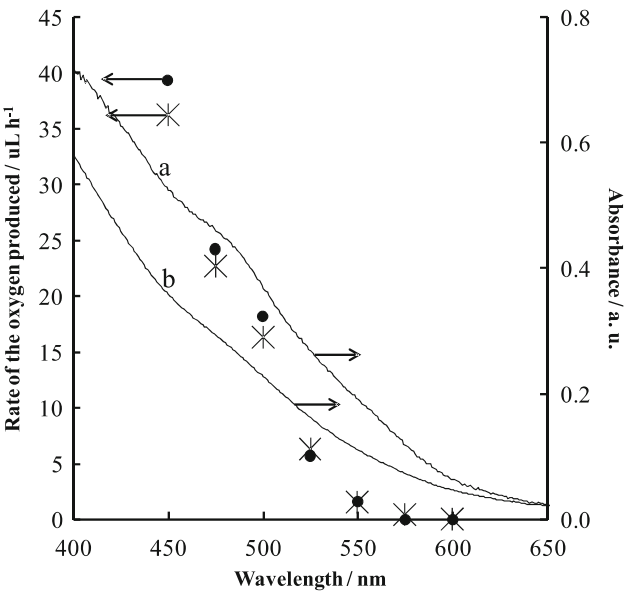

Fig. 8 Action spectra for O_2 evolution in 3 wt% HT-Fe_2O_3/MT (*asterisk*) and 3 wt% HFO/MT (●). The *solid lines* represent the absorption spectra of (a) HFO/MT and (b) HT-Fe_2O_3/MT. When measuring the action spectra for O_2 evolution, the intensity of the monochromatic light was always maintained constant (100 mW cm^{-2}), irrespective of the wavelengths employed. Ag_2SO_4 concentration, 30 mmol dm^{-3} (pH = 6.2); irradiation time, 3 h

saturated loading (25 wt%) in MT, it was found that for a low loading of Fe_2O_3 an amorphous phase can be prepared through calcining. The photocatalytic activity of a polymorph (amorphous or α) was essentially independent of the preparation procedures.

In terms of the photocatalyst loading in MT, it was noted that both Fe_2O_3 and HFO show the most efficient photocatalysis at 3 wt% loading, irrespective of the types of their polymorphs (i.e., α and amorphous phases). In both systems, the water oxidation on photocatalyst surface was the rate-limiting process, and moreover, the kinetics was the same magnitude as the polymorphs employed; in other words, the types of the polymorphs do not kinetically affect the rate-limiting surface reaction. Therefore, as for the appearance of such an optimal photocatalysis condition with the O_2 evolution, this was attributable to a balance between the number of active sites and the hole concentration per the unit surface area. This study first demonstrated the photocatalysis of amorphous Fe_2O_3 comparable with that of α-Fe_2O_3. The utilization of an amorphous compound as photocatalyst is with the merit of the simplicity of its preparation. Thus, particularly in view of green chemistry, it is desirable to aim at creating a highly efficient photocatalysis system by means of amorphous nanoparticles.

References

1. Fujishima A, Honda K (1972) Nature 238:37
2. Leygraf C, Hendewerk M, Somorjai GA (1982) J Phys Chem 86:4484
3. Mohanty S, Ghose J (1992) J Phys Chem Solids 53:81
4. Dare-Edwards MP, Goodenough JB, Hamnett A, Trevellick PR (1983) J Chem Soc Faraday Trans 79:2027
5. Grätzel M, Kiwi J, Morrison LC (1985) J Chem Soc Faraday Trans 1 81:1883
6. Khan SUM, Akikusa J (1999) J Phys Chem B 103:7184
7. Duret A, Grätzel M (2005) J Phys Chem B 109:17184
8. Kennedy JH, Frese KW (1978) J Electrochem Soc 125:709
9. Kay A, Cesar I, Grätzel M (2006) J Am Chem Soc 128:15714
10. Yamanaka S, Doi T, Sako S, Hattori M (1984) Mater Res Bull 19:161
11. Mori H, Miyoshi H, Takeda K, Yoneyama H, Fujita H (1992) J Mater Sci 27:3197. doi:10.1007/BF01116010
12. Miyoshi H, Yoneyama H (1989) J Chem Soc Faraday Trans 85:1873
13. Miyoshi H, Mori H, Yoneyama H (1991) Langmuir 7:503
14. Zhang ZY, Maggard PA (2007) J Photochem Photobiol A 186:8
15. Takahara Y, Kondo JN, Takata T, Lu D, Domen K (2001) Chem Mater 13:1994
16. Feng W, Nansheng D (2000) Chemosphere 41:1137
17. Langford CH, Wong SM, Underdown AW (1981) Can J Chem 59:181
18. Gualtieri A, Venturelli P (1999) Am Mineral 84:895
19. Strehlow WH, Cook EL (1973) J Phys Chem Ref Data 2:163
20. Matsumoto Y (1996) J Solid State Chem 126:227
21. Zboril R, Mashlan M (2002) Chem Mater 14:969
22. He YP, Miao YM, Li CR, Wang SQ, Cao L, Xie SS, Yang GZ, Zou BS, Burada C (2005) Phys Rev B 71:125411.1
23. Esumi K, Yamada K, Sugawara T, Meguro K (1986) Bull Chem Soc Jpn 59:697
24. Enzweiler J, Joekes I (1992) J Colloid Interface Sci 150:559
25. Gondal MA, Hameed A, Yamani ZH, Suwaiyan A (2004) Appl Catal A Gen 268:159
26. Fripiat JJ, Stone WEE (1978) Phys Chem Liq 7:349
27. Itoh K, Bockris JOM (1984) J Appl Phys 56:874